Live fast and die young

Evolution and fate of massive stars

Renzo, M.

Publication date
2019

Document Version
Other version

License
Other

E CIRCUMSTELLAR MATERIAL FROM PULSATIONAL PAIR INSTABILITY

E.1 Resolution study

We present here a study of the impact of the numerical resolution in Lagrangian mass coordinate and time on our results. We refer the interested readers to Marchant et al. (2018) for a study on the relaxation procedure, to Farmer et al. (submitted) for a more comprehensive study of the impact of the numerical resolution and input physics variations on our PPI models, and Renzo et al. (submitted) for a study of the impact of different treatments of time-dependent convection.

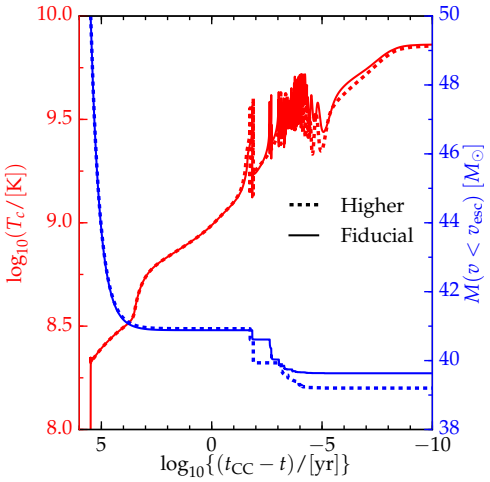

Fig. E.1: Mass (blue, right axis) and central temperature (red, left axis) evolution for our example 50 $M_\odot$ example He core. The scale on the time axis emphasizes the short lived final phases. The differences in the final mass due to variations in the spatial and temporal mesh arise mostly from the dynamical phase of evolution and are limited to $\Delta M \lesssim 0.5\ M_\odot$.

Fig. E.1 shows the evolution in time of the amount of mass bound to the star (blue) and its core temperature (red) for two 50.0 $M_\odot$ He core models computed with different resolutions. `MESA` offers many controls to fine-tune the resolution (see also `inlists` and `run_star_extras.f`), here we vary only three parameters governing the overall variations of averaged quantities across adjacent mesh points and across timesteps. Our fiducial (higher) resolution uses `mesh_delta_coeff=0.8` (`0.6`) and `split_merge_amr_nz_baseline= 8 000` (`10 0000`) for the spatial resolution during the hydrostatic and hydrodynamical phases of evolution, respectively. The time discretization is controlled through `varcontrol_target=5d-5` (`1d-5`). The largest differences in the evolution are found after the onset of the PPI pulses, during the dynamical phase after $\log_{10}\{(t_{\rm CC} - t)/[\mathrm{yr}]\} \lesssim -2$. These result in a $\Delta M = 0.43\ M_\odot$ difference in the mass remaining bound (and on the amount of mass ejected). We emphasize that even our fiducial value provides a resolution significantly higher than the MESA defaults, with a number of mesh points $1289 \lesssim N \lesssim 6311$ and 87900 timesteps from the onset of He core burning to the

onset of core-collapse. For comparison, the higher-resolution model shown in Fig. E.1 has $1583 \lesssim N \lesssim 7908$, however it is able to finish the evolution using a slightly smaller number of timesteps, 86165. This likely indicates that at the higher spatial resolution the most stringent condition on the timesteps is not `varcontrol_target`, and that the higher spatial resolution provides more numerical stability of the solution allowing for longer timesteps.

E.2 Comparison to H-rich model

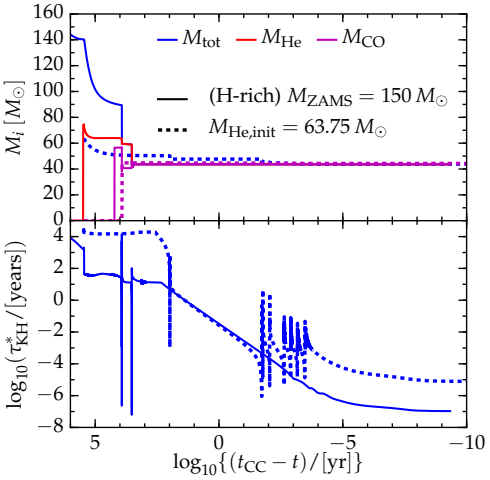

Fig. E.2: Comparison of the evolution of a hydrogen-rich initially 150 $M_\odot$ star (solid lines) to a $M_{\rm He,init} = 63.75\,M_\odot$ core (dashed lines). The He core model is chosen to match the He core mass of the hydrogen-rich star at the end of the main sequence. The top panel shows the total, He, and CO core mass, while the bottom shows the modified thermal timescale of the two models (see Appendix E.2).

A full characterization of PPI+CC evolution for stars with a H-rich envelope is beyond the scope of this study, but we present a brief comparison here. We ran a $M_{\rm ZAMS} = 150\,M_\odot$ hydrogen rich star, assuming $Z = 0.001$ and $Y = 0.27$ for the initial abundance of metals and He, respectively, starting from pre-main sequence to the onset of core collapse. Except for the hydrogen-rich chemical composition, all other parameters are chosen to be identical to those for our naked He cores. This star develops a He core of $M_{\rm He,TAMS} \simeq 63\,M_\odot$ by the end of the main sequence. We compare its evolution to our $M_{\rm He,init} = 63.75\,M_\odot$ model, which is the closest for which we could compute the full evolution in this mass range.

Fig. E.2 compares the evolution of these two models. The top panel shows the evolution of the total mass, the He core mass (corresponding also to the total mass of the He core model), and the CO core mass. The entire hydrogen-rich envelope is indeed ejected at the first pulse at $t_{\rm CC} - t \simeq 10^4$ years (the total mass and the He core mass coincide afterwards), as we expected. Also the final total mass of the stars agree very well, supporting that the evolution of naked He cores is adequate for modeling also the BH masses resulting from hydrogen-rich stars.

However, the locations of the sharp drops in the masses do not correspond exactly, which indicates that the initial presence of a hydrogen-rich envelope can modify the timescale of the pulses. The total number of mass ejection events is two for both of these models, regardless of this. The bottom panel of Fig. E.2 shows the relevant global thermal timescales of the the two stars

$$\tau^*_{\rm KH} = \frac{GM^2_{\rm tot}}{R\mathcal{L}} \quad , \tag{E.1}$$

where $\mathcal{L} = \max\{L, L_\nu\}$. This timescale is sensitive to the stellar radius R, the luminosity L and the neutrino luminosity L_ν (so on the density and temperature structure of the cores), and the total mass $M_{\rm tot}$. The presence of a hydrogen envelope might influence the radial expansion of the He core during a pulse, and thus affect the relevant timescale for relaxation. We emphasize that, during core "bounces" (cf. Paxton et al. 2018 and Sec. 7.5.1), L_ν can vary significantly with a large effect on $\tau^*_{\rm KH}$, however, at this point the evolution of the star is dynamical and not governed by thermal processes. This sensitivity explains the spikes of the dashed line in the bottom panel of Fig. E.2.

E.3 Mass loss per pulse

Table E.1: Number of pulses (pulse), pre-pulse total mass $M_{\rm tot}^{\rm pre-pulse}$, amount of mass lost in the pulse $\Delta M_{\rm pulse}$, time beginning of the pulse $t_{\rm pulse\ start}$ and its duration $\Delta t_{\rm pulse}$ (so that $t_{\rm pulse\ end} = t_{\rm pulse\ start} + \Delta t_{\rm pulse}$, cf. Fig. 7.8), and the velocity of the center of mass of the ejected layers $\langle v \rangle$. The times are defined in Sec. 7.5.3. We list only a representative subset of PPI+CC models.

$M_{\rm He,init}$ $[M_\odot]$	pulse	$M_{\rm tot}^{\rm pre-pulse}$ $[M_\odot]$	$\Delta M_{\rm pulse}$ $[M_\odot]$	$t_{\rm pulse\ start}$ [yr]	$\Delta t_{\rm pulse}$ [hours]	$\langle v \rangle$ $[10^3 {\rm km\ s^1}]$
42.50	1	35.51	9.60×10^{-3}	3.20×10^5	1.26	1.97
43.50	1	36.23	1.52	3.18×10^5	1.05×10^2	3.87
44.50	1	36.95	5.35×10^{-2}	3.16×10^5	3.78	1.72
45.50	1	37.67	8.64×10^{-2}	3.14×10^5	8.51	1.57
46.50	1	38.39	2.65×10^{-2}	3.13×10^5	9.71	1.40
47.50	1	39.10	4.40×10^{-1}	3.11×10^5	3.00×10^1	1.64
48.00	1	39.45	6.11×10^{-1}	3.11×10^5	5.07×10^1	1.78
49.00	1	40.17	1.08	3.09×10^5	1.52×10^2	1.63
50.00	1	40.88	1.24	3.07×10^5	1.27×10^2	1.67
51.00	1	41.58	3.98×10^{-1}	3.06×10^5	3.02×10^1	2.21
	2	41.18	1.61	3.06×10^5	1.58×10^1	1.45
53.50	1	43.33	1.41	3.02×10^5	2.80×10^2	1.99
55.25	1	44.55	3.17×10^{-1}	3.00×10^5	2.86	2.19
	2	44.23	7.80×10^{-1}	3.00×10^5	2.82×10^2	1.85
	3	43.45	2.53×10^{-1}	3.00×10^5	4.85×10^1	1.49
56.50	1	45.42	6.42×10^{-1}	2.98×10^5	6.19	2.14
	2	44.77	7.50×10^{-1}	2.98×10^5	9.11×10^1	1.48
58.50	1	46.79	1.08	2.96×10^5	3.36×10^1	2.15
	2	45.71	1.70	2.96×10^5	1.50×10^2	1.63
59.50	1	47.48	1.31	2.94×10^5	3.63×10^1	2.18
	2	46.17	1.04	2.94×10^5	1.47×10^2	1.71

Continued on next page

$M_{\mathrm{He,init}}$ $[M_\odot]$	pulse	$M_{\mathrm{tot}}^{\mathrm{pre-pulse}}$ $[M_\odot]$	$\Delta M_{\mathrm{pulse}}$ $[M_\odot]$	$t_{\mathrm{pulse\ start}}$ [yr]	$\Delta t_{\mathrm{pulse}}$ [hours]	$\langle v \rangle$ $[10^3 \mathrm{km\ s^1}]$
60.25	3	44.19	4.73×10^{-1}	2.94×10^{5}	6.90	1.70
	1	48.00	1.38	2.93×10^{5}	3.76×10^{1}	2.18
	2	46.61	1.80	2.93×10^{5}	2.28×10^{2}	1.66
	3	44.24	1.81×10^{-2}	2.93×10^{5}	6.15×10^{-1}	1.73
63.75	1	50.34	2.66	2.90×10^{5}	8.39×10^{1}	2.39
	2	47.67	1.56	2.90×10^{5}	1.47×10^{2}	1.51
65.75	1	51.66	3.44	2.89×10^{5}	1.87×10^{2}	2.58
	2	48.16	1.16×10^{-2}	2.90×10^{5}	4.28×10^{1}	7.19×10^{-1}
	3	44.89	1.11	2.90×10^{5}	3.24×10^{1}	1.98
69.75	1	54.29	4.20	2.86×10^{5}	3.90×10^{2}	3.86
	2	44.31	4.69×10^{-1}	2.89×10^{5}	2.71×10^{2}	2.34
	3	44.31	1.84	2.89×10^{5}	4.88×10^{2}	2.15
71.50	1	55.42	5.39	2.85×10^{5}	7.80×10^{1}	3.88
	2	49.73	8.12×10^{-3}	2.88×10^{5}	1.34×10^{2}	6.84×10^{-1}
	3	43.06	7.21×10^{-1}	2.88×10^{5}	3.11×10^{1}	2.02
72.50	1	56.07	7.32	2.84×10^{5}	6.56×10^{2}	3.63
	2	48.41	1.30	2.88×10^{5}	2.43×10^{2}	7.15×10^{-1}
	3	41.66	5.45×10^{-1}	2.88×10^{5}	1.00×10^{1}	1.94
75.00	1	57.68	1.35×10^{1}	2.82×10^{5}	1.69×10^{3}	3.34
	2	44.20	5.50	2.82×10^{5}	4.97×10^{7}	8.01×10^{-1}
	3	38.34	1.27	2.88×10^{5}	1.87×10^{2}	2.33
77.00	1	58.96	1.90×10^{1}	2.81×10^{5}	1.11×10^{3}	3.15
	2	39.57	2.26	2.88×10^{5}	1.44×10^{2}	1.02
80.00	1	60.84	4.16×10^{1}	2.80×10^{5}	2.07×10^{4}	2.35
	2	19.03	8.13×10^{-3}	2.90×10^{5}	3.41×10^{-1}	2.55